Iranian Int. J. Sci. ***5****(1), 2004, p.63-76*

Effect of CT Data Upscaling on Permeability Estimation of Carbonate Samples

Hassanzadeh, E., Ghadirian, H.A.,
NIOC- Research Institute of Petroleum Industry, Pazhoheshgah Blvd., KhairAbad, Qom Road, Tehran, Iran. Email: hassanzadehe@ripi.ir
(received: 12/12/2003 ; accepted: 13/4/2004)

Abstract

Permeability is one of the most important characteristics of hydrocarbon bearing formations. An accurate knowledge of permeability provides petroleum engineers with a tool for efficiently managing the production process of a field. Formation permeability is often measured in the laboratory from cores or evaluated from well test data. To carry out this study, 34 core samples from a carbonate oil field located in the south west of Iran have been considered. The Permeability of samples was measured using a PDPK™ apparatus, the porosity of each sample was measured and CT slices were taken in constant intervals across the samples. Thin sections in the horizontal and vertical directions were prepared from the end pieces of the samples and were analyzed by using the optical microscope. CT numbers corresponding to each slice were exported in the form of a spreadsheet. All such spreadsheets that belong to the i^{th} sample, together with porosity and PDPK™ average permeability were called "i^{th} data set". All data sets were considered as training examples of a back propagation artificial neural network, whilst the target was permeability. Validation of the network results was achieved by leaving out some of the data sets and comparing their measured permeabilities with calculated ones. To decrease calculation time, up scaling was applied on CT data by scales of 2:1, 4:1, 8:1, 16:1 and 32:1 and results were compared with each other. A better understanding of the relationship between volume percentage of minerals, porosity, CT scan data and permeability of carbonates is developed from this study.

Keywords: *CT Scanning, Upscaling, Permeability, Carbonate Samples, Artificial Neural Networks.*

Introduction

Acquiring knowledge on formation permeability in carbonate reservoirs has remained one of the fundamental challenges to petroleum engineers. This important piece of information about porous rock provides engineers with the ability to design and manage efficient processes in the development of oil and gas fields. Using coring tools and bringing samples of the pay zone to the surface and measuring their permeability under simulated downhole conditions is one of the oldest practices for estimating the formation permeability. Coring every well in a large field can be very expensive. It is necessary and inevitable to core some wells no matter how small or large a field. On the other hand, trying to get a representative sample from every single well, especially in fields with hundreds of wells, requires a large amount of capital. In a heterogeneous field where permeability values tend to change rapidly with spatial coordinates, such practices (coring every well), although expensive, would provide valuable information. Having a representative value for permeability in different locations, especially where wells (injection or production) are drilled could be used effectively in reservoir simulation studies.

Oil and oil service companies began using CT and MRI imaging technologies in the mid-1980s. The Oil industry uses X-ray Computerized Tomography (CT) and Magnetic Resonance Imaging (MRI) to characterize rock samples (cores) taken from wells (Wellington et al., 1987). The industry is interested not only in topological issues concerning the structure of the rock samples or fluid boundaries; but, it is also essential to quantify the three-dimensional distribution of properties such as density and effective atomic number. CT scan data is widely used to calculate porosity and build 3D models of rock matrix in carbonates, but in this study we illustrate a method to use these data together with conventional laboratory measurements for estimating permeability of carbonate rocks.

During the past several years, the number of successful applications of neural networks to solve complex problems has increased exponentially. Considerable attention has been devoted to the use of neural networks as an alternative approach to interpolation and extrapolation, pattern recognition, statistical, and mathematical

modeling (Murray, 1995). For example, back-propagation neural networks were used to develop process models as substitutes for complicated empirical and mathematical models (Nikravesh, 1994). These models can be used as an alternative to statistical and time series analysis. Neural network analysis, unlike regression, does not require specification of structural relationships between the input and output data. However, identification using neural networks is more useful when large amounts of data are available. Some CT data volumes may consist of 1000×1000×1000 pixels (or voxels) and artificial neural networks could significantly help geoscientists to identify relationships between different types of core properties and CT data (Herman, 1978).

Procedures

Sample Description

This study is carried out on 34 core samples that have been taken from Sarvak Formation in the four exploration wells located in the south west of Iran. The limestones of the overlying Sarvak Formation (Albian – Turonian) formed during the high stand. A major sea-level fall at the Cenomanian– Turonian boundary exposed carbonates of the Sarvak Formation. However, the uppermost portion of the Sarvak Formation was deposited during an early Turonian sea-level rise, and was subsequently exposed due to a minor sea-level fall. Major diagenetic alterations occurred along the Cenomanian - Turonian unconformity. Meteoric processes resulted in karstification, generation of porosity and permeability, and dolomitization, forming good reservoir quality strata in the Sarvak Formation. Burial diagenesis affected all units, in some cases increasing porosity and permeability and in others decreasing them (Kayvani et al., 2002). Investigating correlations between permeability and other petrophysical properties in carbonate rocks is not as straightforward as in sandstones. For example different types of porosity in carbonate rocks such as vugs, micro-fractures, intragranular and intergranular porosity, results in permeability variations for the same porosity. Therefore considering other types of available data to estimate permeability in carbonates could increase accuracy of the results.

The depth of sampling was determined based on petrophysical and geological logs in the four exploration wells. The samples were prepared as cylindrical shape plugs; these samples are plugged vertically and are 1.5" in diameter and 2.5" in length (Figure 1). After preparation of samples, precise physical measurements were taken, (including mass, diameter and length) and then the porosity and permeability of samples were determined. Densities were achieved by calculating mass/volume ratios for each sample, porosities were determined using an ASC300 porosity meter and permeability measured by a pressure decay profile permeametry (PDPK™) apparatus. To measure permeability of samples they were located in the specific place of apparatus and pressure decays were measured in two orthogonal directions (as shown in Figure 1) in 1cm constant intervals along the sample's main axis. Average of all measured values for each core sample is called "Average Horizontal PDPK™ Permeability" of the sample.

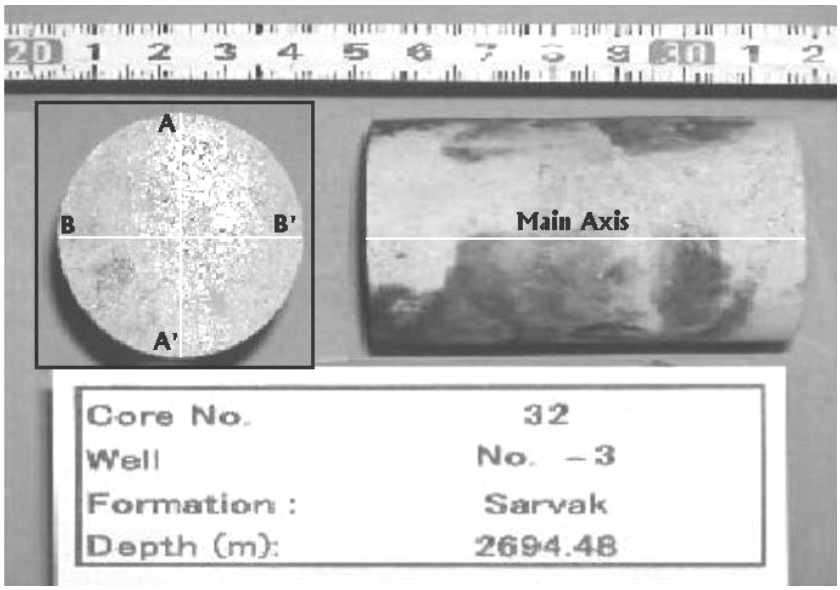

Figure 1. Sample photo-montage of core plugs.

Scanning Procedure

An Xforce Toshiba CT scanner (third generation) was used in this study. The scanner consists of a mainframe, rotational elements, and scanner electronics. The mainframe houses the X-ray source, detector array, and beam shaping elements. The scanner assembly consists of a

support table for positioning the core. The generator group is responsible for generating the X-rays. The control panel consists of a video console, an interactive keyboard for viewing, initiating image generation, and for image manipulation. The computation unit performs sequencing, interprets instructions, and executes them. The Image Processing System accepts image information in digital form and converts it to the image seen on the viewing monitors. Processed images including digital data have been stored in appropriate storage media such as magnetic disks (Hounsfield, 1972).

The cores were initially cleaned, dried and then scanned at room pressure and temperature at an energy level of 120 keV and a field size of 18 cm. A small field of scan was used to obtain better spatial resolution, as the number of pixels available remains constant. Slices were taken in 2 mm constant intervals along each sample as it is displayed in Figure 2. Table 1 shows the CT value of representative minerals.

Slice thickness was made as small as possible, i.e., 1 mm (it varies from 1-10 mm), in order to minimize errors and maximize resolution. Greater slice thickness results in greater measurement error. The size for each CT slice is 112×112, and each pixel represents a volume of 0.35 mm×0.35 mm×1 mm. The average CT value within each pixel has been considered as CT value of the pixel. Figure 3 shows a series of CT images obtained for each core sample.

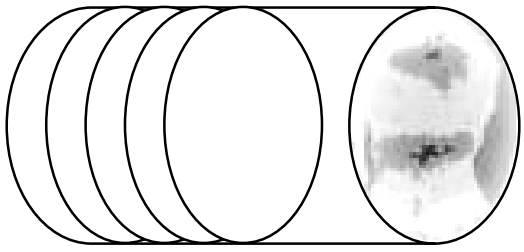

2 mm

Figure 2. Schematic of the CT slices along the sample.

Table 1. Linear attenuation coefficients (μ) and CT numbers for some common mineral end-members. The tabulated values are calculated specifically for 120keV X-ray energy (modified from University of Texas's web site).

Mineral Name	Idealized Formula	Mass Density (g/cm^3)	μ (cm^{-1})	CT Number (HU)
Quartz	SiO_2	2.65	0.448	1275
Muscovite	$KAl_3Si_3O_{10}(OH)_2$	2.83	0.490	1323
Hedenbergite	$CaFeSi_2O_6$	3.63	0.823	2005
Calcite	$CaCO_3$	2.71	0.530	1384
Dolomite	$CaMg(CO_3)_2$	2.87	0.513	1357
Microcline	$KAlSi_3O_8$	2.56	0.452	1279
Rutile	TiO_2	4.25	0.955	2326
Diopside	$CaMgSi_2O_6$	3.23	0.601	1513
Albite	$NaAlSi_3O_8$	2.62	0.436	1266
Fayalite	Fe_2SiO_4	4.39	1.22	2993
Magnetite	Fe_3O_4	5.22	1.62	4000

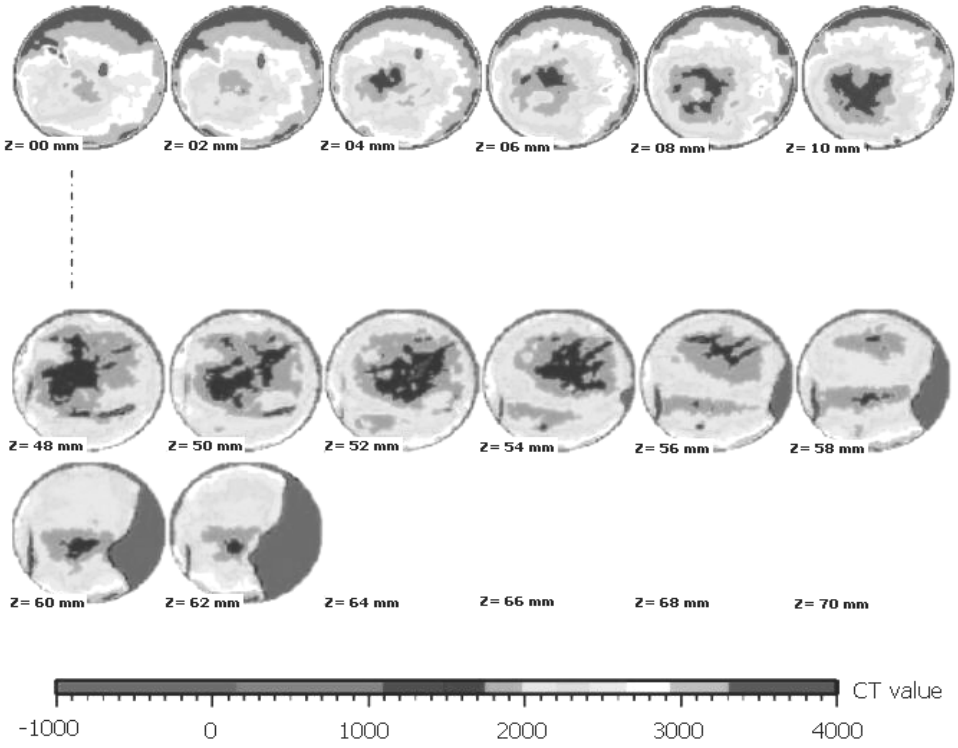

Figure 3. A series of CT images obtained for core samples.

Data Set Arrangement

CT data of a core sample consists of 32 matrices each of 112×112 size which in mathematical notation can be showed as CT(i,j) & i,j=

1,2,…,112. To reduce size of CT data and consequently calculation time, the average of each CT slice has been considered as representative of that slice. In this study we considered 6 data sets of different scales for each sample. First set consists of 32 CT slice averages together with porosity, depth of samples, bulk density and volume percentage of minerals as input , and permeability of samples as output part of data. The second, third, forth and fifth data sets consist of all information of first data set, but the difference is in scale of CT data. The number of CT averages has been reduced by scales of 1/2, 1/4, 1/8 , 1/16 and 1/32 as shown in figure 4.

Up scaling the CT averages is done using a simple averaging method:

$$A_k^{[32]} = (\sum_{i,j} CT(i,j))/12544 \quad k = 1,2,\ldots,32 \text{ (Slice No.) \& } i,j = 1,2,\ldots,112$$

$$\begin{aligned} A_l^{[16]} &= (A_{2l}^{[32]} + A_{2l-1}^{[32]})/2 \qquad l = 1,2,\ldots,16 \\ A_l^{[8]} &= (A_{2l}^{[16]} + A_{2l-1}^{[16]})/2 \qquad l = 1,2,\ldots,8 \\ A_l^{[4]} &= (A_{2l}^{[8]} + A_{2l-1}^{[8]})/2 \qquad l = 1,2,3,4 \\ A_l^{[2]} &= (A_{2l}^{[4]} + A_{2l-1}^{[4]})/2 \qquad l = 1,2 \\ A^{[1]} &= (A_1^{[2]} + A_2^{[2]})/2 \end{aligned} \tag{1}$$

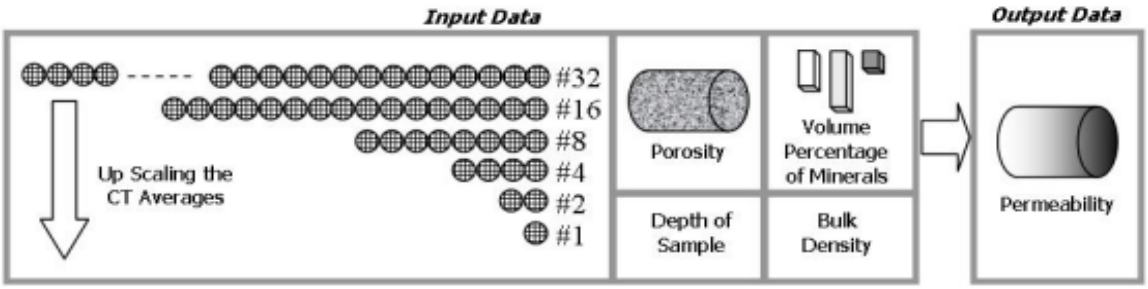

Figure 4. Schematic of data sets.

Neural Network Structure

Known as sixth generation computing, neural networks are widely used in many disciplines from weather forecast to airport security devices. Neural networks are analog, distributive and parallel information processing methods that have proven to be powerful pattern recognition tools (Fausett, 1994). Since they process data and learn in a parallel and distributed fashion, they are able to discover highly complex relationships between several variables that are

presented to the network. As a model-free function estimator, neural networks can map input to output no matter how complex the relationship. There are several paradigms that can be used to generate neural networks. To achieve the goal of this study, a feed forward, back propagation neural network (which adopts a supervised training scheme) has been used. An artificial neural network is a system of several simple processing units known as nodes, neurons or processing elements. These processing elements are associated with one another through simple connections known as synaptic connections. The strength of the synaptic connections changes with attaching a weight to them. Figure 5 is a schematic diagram of a typical artificial neural network.

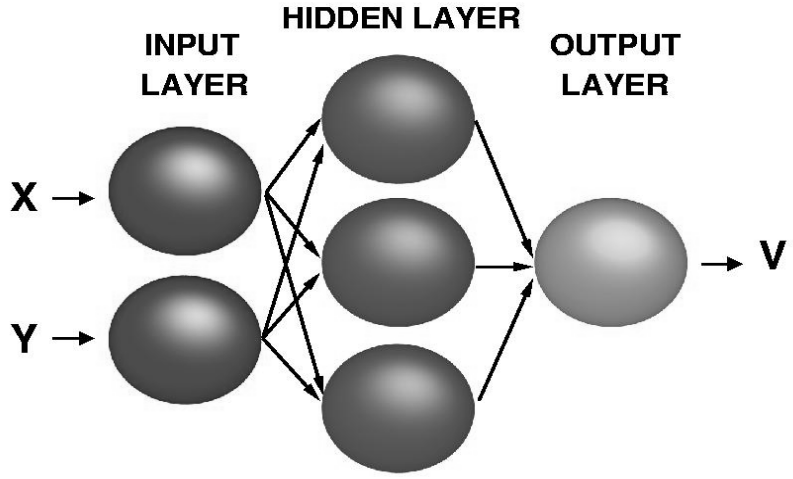

Figure 5. Schematic of an Artificial Neural Network.

Neurons in a network are organized in layers. Each layer is responsible for a particular task. Typically there are three kinds of layers in an artificial neural network. Input layer is responsible for presenting the network with the necessary information from the outside world in a normalized manner. Hidden layers (there may be more than one hidden layer in a network, this is a problem dependent factor) contain hidden neurons that are responsible for the main part of the input to output mapping. These neurons are responsible for feature extraction from the input neurons and subsequently passing the information to the output neurons. Output layer contains output neurons that communicate the outcome of the neural networks

computation with the user. The back-propagation learning rule that is used in this study is introduced by Bishop (1996).
A processing element of a feed-forward network transfers its inputs as follows:

$$X_j^{[s]} = f(\sum_i (W_{ji}^{[s]} \cdot X_j^{[s-1]})) = f(I_j^{[s]}) \quad (2)$$

where f is a transfer function. The function f can be any smooth function for a processing element. The sigmoid function is used as the transfer function in this study. After selecting neural network structure, samples for training and testing the network are collected as described in Figure 5. During the supervised training, it was necessary to provide the network with the correct permeability value for each example. The network will converge to the correct permeability value by back propagating the error between its prediction and the actual permeability value.

Results

Figure 6 shows the relationship between sample permeability and CT average, depth, percentages of calcite, and dolomite, respectively. The scatter of these plots and low correlation coefficients (except for CT average that is a function of density) suggest no apparent relationship between these parameters and formation permeability.

Samples were divided into two sets, one set containing 22 samples for analysis or learning and another set of 12 samples for testing of the results. We performed multiple linear regressions on the analysis data set to achieve a general formula for calculating permeability using other available parameters of the samples as shown in Figure 7. The correlation coefficient is moderate. Figure 8 is a comparison between the actual permeability of test samples and calculated values. The correlation coefficient is good. The networks were trained and then tested to see if they were able to estimate/predict permeability values from the four wells in Sarvak formation. The 12 samples that were chosen randomly in this study for test purposes (and were never seen by networks during the training) included a wide range of permeabilities from 0.05 to 179.15 mD. This further indicates the high degree of heterogeneity of this formation. Figure 9 shows the actual

permeability values of test samples that were measured in the laboratory in comparison with the network's estimation/prediction for each sample. Although permeability values cover a wide range, the network is able to follow the trend very closely. This figure show's an increase in accuracy of predictions as the number of CT averages (NN CT [#]) is increased, especially for the samples with low permeability. After plotting core measurements versus network predictions, one can see the divergence of the predictions from a perfect match, which is the unit slope line. Figure 10 displays effect of up scaling the CT averages on permeability prediction. Comparing the results presented in Figures 9 and 10 with that of Figures 8 and 7 reveals the power of artificial neural networks in pattern recognition. One might comment on the input variables that were used in this study in the following fashion: CT numbers are related to the density, topology and structure of medium and consequently are related to the fractures that have doubtless influence on permeability. Depth of the formation is an indication of reservoir pressure that might affect permeability. Percentage of minerals cause changes in wettability which has a direct impact on permeability.

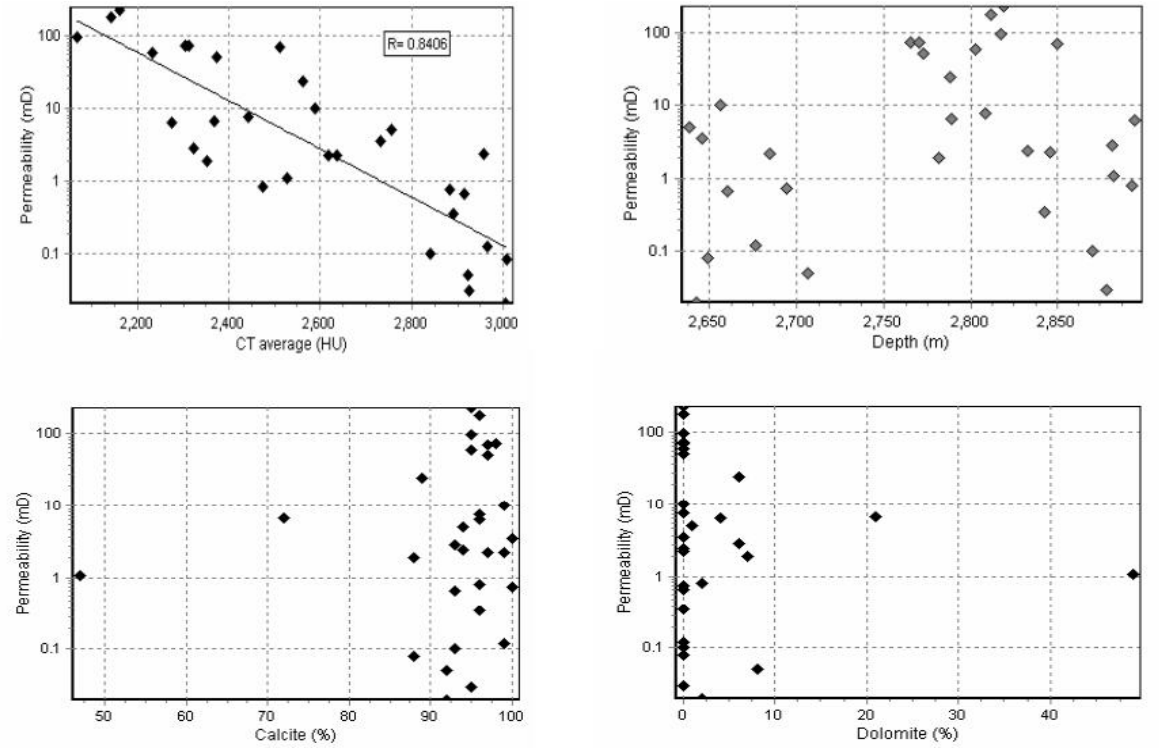

Figure 6. Relationships between permeability with other data of samples.

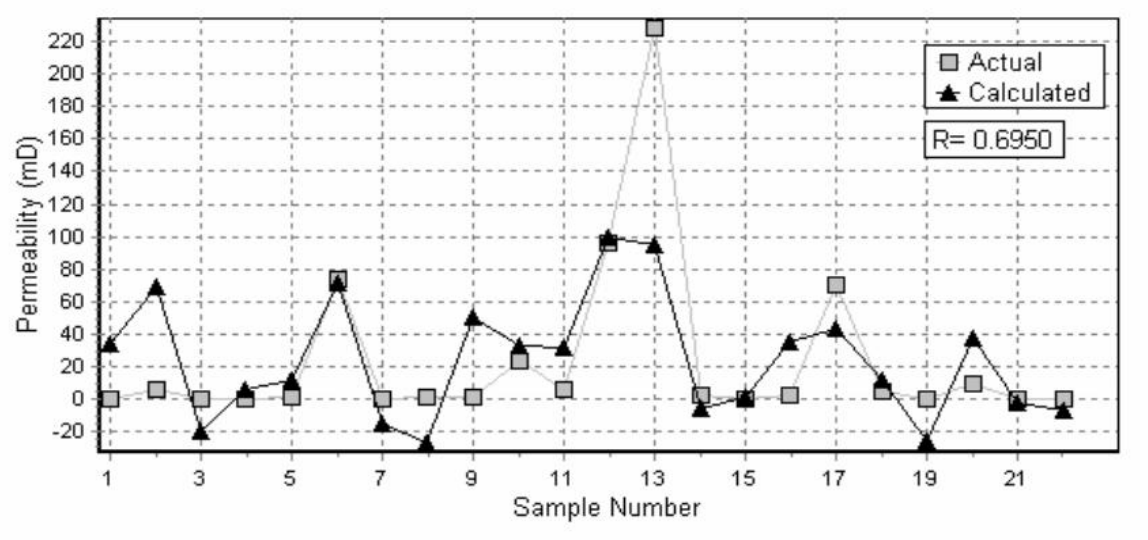

Figure 7. Comparison between measured with calculated permeability values of 22 core samples obtained from multiple linear regression.

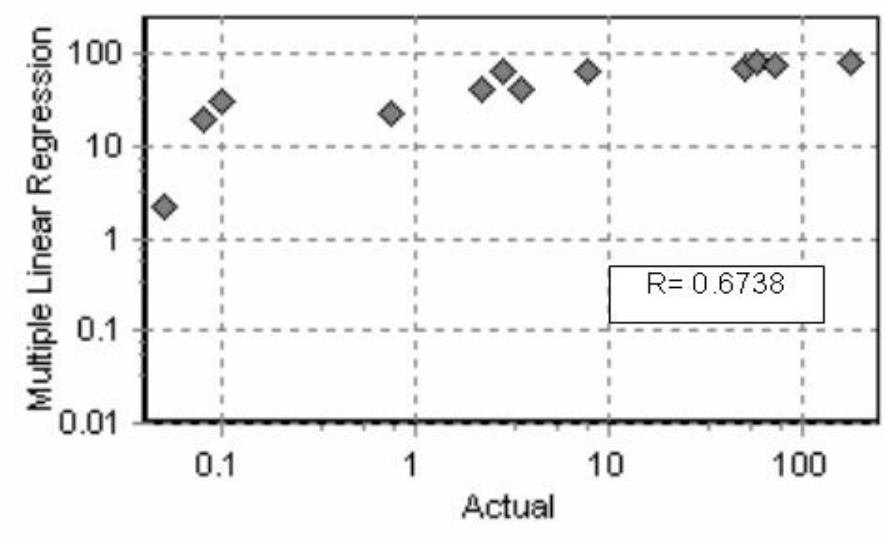

Figure 8. Cross plot of measured and calculated permeability values of 12 test samples obtained from multiple linear regression.

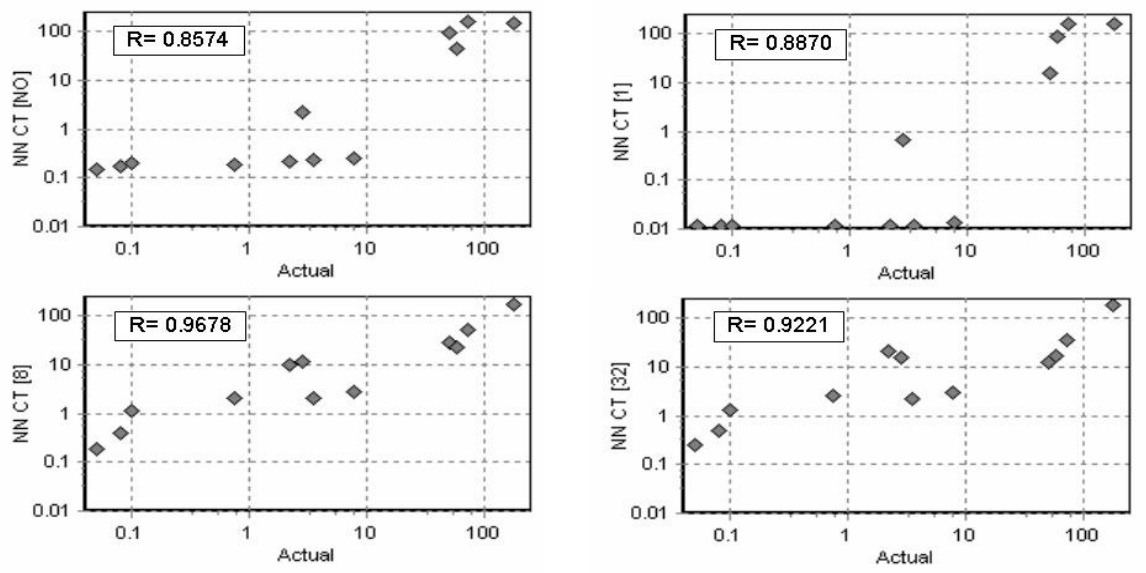

Figure 9. Comparison between results of ANNs containing different numbers of CT averages.

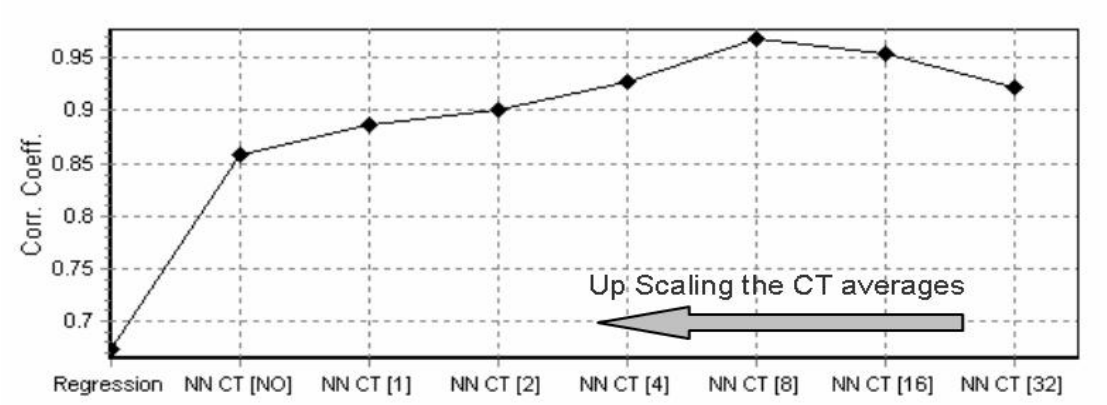

Figure 10. Effect of CT data Upscaling on Permeability prediction.

Discussion

The results presented here are based on data of 34 samples taken from four exploration wells. A few points about these results need to be mentioned. Our experience with the design and development of neural networks for permeability prediction/estimation has shown that it is essential to have enough data to train the network properly in order to see acceptable, as well as repeatable, results. The questions of how much data is enough and whether there exists a threshold below which neural nets will not be effective are currently under investigation. The

results are as good as the data available. With proper data more can be done with neural networks than any other tool.

Conclusions

This study showed that neural network estimation of carbonates permeability using other laboratory data is a feasible methodology. Artificial neural networks that are capable of predicting/estimating carbonate permeability using other available data, were presented. It was shown that the trained networks were able to predict/estimate permeability comparable to that of actual core measurements. Availability of reliable core data for training process proved to be essential. At this point, this type of study is capable of producing lab specific results, however, additional data on seize and distribution of fractures and also porosity type, could help us to find relationships between CT data scale and permeability. Adequate knowledge on fundamental theories and practices of artificial neural networks are required to achieve acceptable and repeatable results.

Nomenclature

μ = linear attenuation coefficient, L^{-1}, cm^{-1}
CT = Computed Tomography number
HU = Hounsfield unit
R = linear correlation coefficient
$X_j^{[s]}$ = output state of j^{th} node in layer s
$W_{ji}^{[s]}$ = connection weight joining i^{th} node in layer (s-1) to j^{th} node in layer s
$I_j^{[s]}$ = weighted summation of inputs to j^{th} node in layer s
f = transfer function
NN CT[i] = set of neural net predictions using i number of CT averages

References

Bishop, M.C., and Bishop, C., (1996) *Neural Networks for Pattern Recognition*, Oxford University Press, USA, PP. 116-160.

Fausett, L. (1994) *Fundamentals of Neural Networks*, Prentice-Hall, USA, PP. 289-330.

Herman, G.T. (1978) *An Introduction to Some Basic Mathematical Concepts of Computed Tomography*, Roentgen-Video-Techniques for Dynamic Studies, Ed. P. heintzen and J. Bursch, Georg Thieme Publishers, Stuttgart, Germany, PP. 253-260.

Hounsfield, G.N. (1972) *A Method of an Apparatus for Examination of a Body by Radiation Such as X-ray or Gamma Radiation*, U.K. Patent No.1283915.

Kayvani, F., and Heydari, E. (2002) *Depositional environments and diagenesis of cretaceous (albian to maasterichtian) strata of the Abadan plain of the Persian platform in southwestern of Iran*, Proceedings of The Geological Society of America Annual Meeting, Denver, CO.

Murray, A.F. (1995) *Applications of Neural Networks,* Kluwer Academic Publishers, Boston, PP. 129-150.

Nikravesh, M. (1994) *Dynamic Neural Network Control*, Ph.D. Dissertation, University of South Carolina, Columbia, SC.

Wellington, S.L., and Vinegar, H.J. (1987) *X-ray Computerized Tomography*, Journal of Petroleum Technology, **8,** 885-898.